Effect of long-range order on elastic properties of $Pd_{0.5}Ag_{0.5}$ alloy from first principles

E. K. Delczeg-Czirjak,[1] E. Nurmi,[2,3,4] K. Kokko,[2,4] and L. Vitos[1,5,6]

[1]*Applied Materials Physics, Department of Materials Science and Engineering, KTH Royal Institute of Technology, SE-100 44 Stockholm, Sweden*

[2]*Department of Physics and Astronomy, University of Turku, FI-20014 Turku, Finland*

[3]*Graduate School of Materials Research, Turku, Finland*

[4]*Turku University Centre for Materials and Surfaces (MatSurf), Turku, Finland*

[5]*Division for Materials Theory, Department of Physics and Materials Science, Uppsala University, SE-75120 Uppsala, P. O. Box 516, Sweden*

[6]*Research Institute for Solid State Physics and Optics, H-1525 Budapest, P.O. Box 49, Hungary*

(Received 30 June 2011; published 21 September 2011)

The effect of long-range order on single-crystal elastic constants of $Pd_{0.5}Ag_{0.5}$ alloy has been investigated using first-principles electronic structure calculations. The lowest energy among the considered ordered, partially ordered, and disordered structures is found to be the $L1_1$ layered structure, which is formed by alternate (111) Pd and Ag layers. The ordering effect is found to follow a clear trend: in contrast to the disordered phase, for which the K_a and K_c compressibilities are equal, the $L1_1$ structure becomes less compressible along the c axis than along the a axis.

DOI: 10.1103/PhysRevB.84.094205 PACS number(s): 71.15.Nc, 62.20.D−, 71.20.Be, 81.05.Bx

I. INTRODUCTION

According to the experimental phase diagram,[1] Pd and Ag form a continuous solid solution within the face-centered-cubic (fcc) crystallographic phase. The random alloys show many interesting features as a function of concentration; several physical quantities have nonmonotonic or discontinuous character. The electronic topological transitions (ETT) have been predicted to affect the physical properties.[2–4] At low temperatures, three ordered structures have been suggested: the $L1_2$ (Cu_3Au-type) structure for Pd_3Ag, the $L1_1$ (CuPt-type) structure for equiatomic Pd-Ag, and the $L1_1^+$ structure for $PdAg_3$.[5]

Our previous work deals with a systematic study of the concentration dependence of the single- and polycrystalline elastic constants of random $Pd_{1-x}Ag_x$ alloys.[4] Using an *ab initio* method based on density functional theory,[6] we have shown that the elastic constants of random fcc solid solutions do not follow the simple linear-mixing law as a function of composition. The employed chemically random structure is definitely an appropriate description of the $Pd_{1-x}Ag_x$ alloys at high temperatures, but the physical state at low temperatures might be different, as suggested by recent investigations.[5,7] The ordering in turn may have a marked impact on the bulk properties of Pd-Ag system.

In the present work, we focus on the ordering effect on the elastic properties of $Pd_{0.5}Ag_{0.5}$ alloy. Considering different degrees of long-range order, we study how the elastic parameters change from the completely disordered phase to the ordered lattice predicted by theory.[5] The $L1_1$ structure is a layered structure formed below 320 K, in which the Pd and Ag monolayers alternate along the [111] direction of the fcc lattice $[(Pd)_1/(Ag)_1]$. The structure can be represented with a hexagonal lattice, having the c axis along the cubic [111] direction and with 6 atoms per hexagonal unit cell. The single-crystal elastic constants of $Pd_{0.5}Ag_{0.5}$ alloy are calculated within the hexagonal representation as a function of the degree of ordering. The results obtained are compared with the previously calculated elastic constants of the substitutionally disordered fcc-type structure of $Pd_{0.5}Ag_{0.5}$.[4] The degree of long-range order in the $L1_1$ structure is controlled by modifying the layer composition; namely, considering a layered structure along the [111] direction in the cubic lattice with composition $(Pd_{1-x}Ag_x)/(Pd_xAg_{1-x})$ and changing x from 0.5 (corresponding to the completely disordered system) to 1 (corresponding to the completely ordered system). We demonstrate that, in this particular case, the long-range order does not significantly affect the single-crystal elastic constants, sustaining that the random fcc solid solution model is accurate enough even at low temperatures.

The rest of the paper is divided in two main sections and conclusions. Sec. II presents the theoretical tools. This includes a brief overview of the *ab initio* electronic structure method and the theory of the elastic constants, and the most important details of the numerical calculations. The results are presented and discussed in Sec. III. In the Appendix the Euler rotation matrix connecting the hexagonal and cubic representations of the disordered system is presented.

II. THEORETICAL TOOLS

A. Total energy method

The electronic structure and total energy calculations have been carried out using the exact muffin-tin orbitals (EMTO) method.[8–12] The EMTO method is an efficient and accurate tool for solving the Kohn-Sham equations.[13] It can be considered as an improved Korringa-Kohn-Rostoker (KKR) method, where the exact Kohn-Sham potential is represented by large overlapping potential spheres. Inside these spheres the potential is spherically symmetric and constant between the spheres. Within the EMTO method the one-electron states are determined exactly (within the common numerical errors) for an optimized overlapping muffin-tin potential. This potential is chosen as the best possible spherical approximation to the exact potential:[9,12,14] the radii of the potential spheres, the spherical potential waves, and the constant value from the interstitial, are calculated by minimizing (a) the deviation

between the exact and overlapping potentials and (b) the errors coming from the overlap between the spheres.

The compositional disorder in alloys is treated using the coherent potential approximation[15,16] and the total energy is computed via the full charge-density technique.[17] It was shown in a number of previous investigations that the EMTO method is suitable and sufficiently accurate to compute the anisotropic lattice distortions and thus the elastic constants in random alloys.[11,12,18–24] A full description of the EMTO method may be found in Refs. [8–12].

B. Elastic properties

The elastic properties of single crystals are described by the elements c_{ij} of the elasticity tensor. For a hexagonal lattice there are five independent elastic constants, c_{11}, c_{12}, c_{13}, c_{33} and c_{44}, according to Voigt's notation. The energy change upon a general strain is given by

$$\frac{1}{V}\Delta E = \tfrac{1}{2}c_{11}\left(e_1^2+e_2^2\right)+c_{33}e_3^2+c_{12}e_1e_2+c_{13}(e_2e_3+e_1e_3) + \frac{1}{2}c_{44}\left(e_4^2+e_5^2\right)+\frac{1}{2}c_{66}e_6^2+O(e^3), \tag{1}$$

where $c_{66}=(c_{11}-c_{12})/2$, V is the volume of the system, and e_i are the elements of the strain matrix.

The relations between c_{11}, c_{12}, c_{13}, and c_{33} are given by the bulk modulus B and the dimensionless quantity R as follows:

$$B=\frac{c_{33}(c_{11}+c_{12})-2c_{13}^2}{c_s} \tag{2}$$

and

$$R=\frac{c_{33}-c_{11}-c_{12}+c_{13}}{c_s}, \tag{3}$$

where c_s is given by

$$c_s \equiv c_{11}+c_{12}+2c_{33}-4c_{13}. \tag{4}$$

Due to the lower symmetry of the investigated layered structures, their hexagonal axial ratio c/a may change with volume. The volume dependence of the equilibrium hexagonal axial ratio $[(c/a)_0(V)]$ is related to the difference in the linear compressibilities along the a (K_a) and c (K_c) axes, given by the dimensionless quantity R:

$$R=B(K_a-K_c)=-\frac{d\ln(c/a)_0(V)}{d\ln V}. \tag{5}$$

The ratio of the direction-dependent compressibilities is given by[22]

$$\frac{K_a}{K_c}=\frac{c_{11}+c_{12}-2c_{13}}{c_{33}-c_{13}}. \tag{6}$$

c_s is obtained from the second-order derivative of $E(V,c/a)$:

$$c_s=\frac{9(c/a)_g^2}{2V_g}\left.\frac{\partial^2E(V_g,c/a)}{\partial(c/a)^2}\right|_{c/a=(c/a)_g}, \tag{7}$$

where $(c/a)_g$ is the global equilibrium c/a ratio $(c/a)_0(V_g)$, where V_g stands for the equilibrium volume. Finally, c_{44} (c_{66}) is determined from a monoclinic (orthorhombic) strain as described in Eq. (11).

For the disordered phase, the cubic and hexagonal structures are equivalent. In order to be able to compare the present elastic parameters to the previously calculated parameters,[4] we need to make a transformation from the cubic to hexagonal coordinate system. The relation between the fcc (c_{ij}^{F}) and hexagonal (c_{ij}^{H}) elastic constants are given by the tensor transformation rules, according to which

$$c_{ijkl}^{\mathrm{H}}=\sum_{m,n,o,p=1}^{3}T_{im}T_{jn}T_{ko}T_{lp}c_{mnop}^{F}, \tag{8}$$

where $T_{\alpha\beta}$ ($\alpha=ijkl$ and $\beta=mnop$) are the elements of the tensor transformation matrix T (see Appendix). For the present case, we have

$$T=\begin{pmatrix}-\frac{\sqrt{2}}{2} & \frac{\sqrt{2}}{2} & 0\\ -\frac{\sqrt{6}}{6} & -\frac{\sqrt{6}}{6} & \frac{\sqrt{6}}{3}\\ \frac{\sqrt{3}}{3} & \frac{\sqrt{3}}{3} & \frac{\sqrt{3}}{3}\end{pmatrix}. \tag{9}$$

After some algebra we arrive at

$$\begin{aligned} c_{11}^{\mathrm{H}}&=\left(c_{11}^F+c_{12}^F+2c_{44}^F\right)/2,\\ c_{12}^{\mathrm{H}}&=\left(c_{11}^F+5c_{12}^F-2c_{44}^F\right)/6,\\ c_{13}^{\mathrm{H}}&=\left(c_{11}^F+2c_{12}^F-2c_{44}^F\right)/3,\\ c_{33}^{\mathrm{H}}&=\left(c_{11}^F+2c_{12}^F+4c_{44}^F\right)/3,\\ c_{44}^{\mathrm{H}}&=\left(c_{11}^F-c_{12}^F+c_{44}^F\right)/3. \end{aligned} \tag{10}$$

We emphasize that these relations are valid only for the disordered phase.

C. Details of numerical calculations

The one-electron equations are solved within the soft-core and scalar-relativistic approximations. The Green's function is calculated for 16 complex energy points distributed exponentially on a semicircular contour including states within 1 Ry below the Fermi level. In the basis set we include s, p, d, and f orbitals and, in the one-center expansion of the full charge density, we used cutoff $l_{\max}^h=8$. The electrostatic correction to the single-site coherent-potential approximation is described using the screened impurity model[25] with a screening parameter of 0.9. The self-consistent EMTO calculations are performed within the local-density approximation (LDA)[26] for the exchange-correlation functional. Our previous work[4] shows that the best agreement between the theoretical and experimental bulk properties are given by the revised version of the Perdew-Burke-Ernzerhof exchange correlation approximation for solids and surfaces (PBEsol).[27] Therefore, the total energies are calculated with PBEsol via the full charge-density technique. A detailed discussion about the accuracy of the method used and the chosen exchange-correlation functional can be found in Sec. III A of Ref. 4.

To derive the elastic parameters, the total energy is calculated for six different volumes and, for each volume, seven different c/a ratios are used. This procedure yields to a two-dimensional total energy surface $E=E(V,c/a)$.

The derivatives appearing in the formulas of elastic quantities [Eqs. (5) and (7)] are obtained by fitting the calculated

$E(V,c/a)$ data. For R, the volume-dependent c/a minimum $[(c/a)_0(V)]$ is obtained using a second-order polynomial fit. This also defines an energy minimum for each volume at $(c/a)_0(V)$, which is denoted by $E(V,(c/a)_0)$. Fitting a Morse-type equation of state to $E(V,(c/a)_0)$ versus V we obtain the global energy minimum (E), the bulk modulus, and the equilibrium volume (V_g), expressed here by the Wigner-Seitz radius r_{WS}. $(c/a)_0(V_g)$ gives the global equilibrium c/a value $[(c/a)_g]$. c_s in turn is obtained from the second-order derivative of $E(V,c/a)$ calculated according to Eq. (7) at $(c/a)_g$ and V_g.

In order to calculate c_{66} and c_{44} we use the following volume-conserving orthorhombic and monoclinic deformations:

$$\begin{pmatrix} 1+\varepsilon_{\mathrm{o}} & 0 & 0 \\ 0 & 1-\varepsilon_{\mathrm{o}} & 0 \\ 0 & 0 & \frac{1}{1-\varepsilon_{\mathrm{o}}^2} \end{pmatrix} \text{ and } \begin{pmatrix} 1 & 0 & \varepsilon_{\mathrm{m}} \\ 0 & \frac{1}{1-\varepsilon_m^2} & 0 \\ \varepsilon_{\mathrm{m}} & 0 & 1 \end{pmatrix}, \quad (11)$$

respectively, applied on the hexagonal unit cell. The corresponding distorted structures are described as base-centered orthorhombic and simple-monoclinic lattices, respectively. The total energies, $E(\varepsilon_{\mathrm{o}}) = E(0) + 2Vc_{66}\varepsilon_{\mathrm{o}}^2 + O(\varepsilon_{\mathrm{o}}^4)$ and $E(\varepsilon_{\mathrm{m}}) = E(0) + 2Vc_{44}\varepsilon_{\mathrm{m}}^2 + O(\varepsilon_{\mathrm{m}}^4)$, are computed for six distortions $\varepsilon = 0.00, 0.01, \ldots, 0.05$.

To obtain the accuracy needed for the calculation of $E(V,c/a)$ (c_{44} and c_{66}) 1000 (5000) uniformly distributed k points are used in the irreducible wedge of the Brillouin zone.

Previous *ab initio* calculations show that the effect of the local lattice relaxation (LLR) on the elastic parameters remains small even if a large size mismatch exists between the alloy components. In particular, it was shown that the LLR effect is almost negligible for the bulk modulus of Fe-based binary alloys[28] and also for the tetragonal shear modulus c' of $Al_{0.95}Li_{0.05}$ alloy.[18] Therefore, in the present study the effect of the local lattice relaxation is neglected.

III. RESULTS

The bulk properties and single-crystal elastic constants of $Pd_{0.5}Ag_{0.5}$ are calculated for three different phases: (i) the completely disordered phase (labelled H_d), where the Pd and Ag atoms are distributed with equal probabilities within the layers of the $L1_1$ structure, (ii) the partially ordered phase (H_{po}), where the Pd and Ag atoms are mixed with certain probabilities (20% of Ag in a Pd layer and vice versa) within the layers, and (iii) the ordered phase (H_o), which stands for the layered structure where the different types of atoms occupy alternating layers. In the following tables, F_d stands for the results from Ref. 4 obtained for the completely disordered phase represented by an fcc lattice. For completeness, we also transformed the cubic results to the hexagonal lattice (denoted by F_d^H).

A. Accuracy

In the ideal case, the results for H_d should coincide with those for F_d. As Table I shows, the differences between the H_d and F_d data are 0.01% for the Wigner-Seitz radius (r_{WS}) and global equilibrium c/a, 0.17% for the bulk modulus, and 0.077 mRy for the total energy per site (E). These differences are expected to be mainly due to the different numerical implementations (e.g., Brillouin zone sampling) corresponding to different crystal symmetries.

TABLE I. Effect of different structural representations on calculated results. Theoretical (EMTO-PBEsol) results are presented for $(c/a)_g$, r_{WS}, B, E, R, c_s, and single-crystal elastic constants of $Pd_{0.5}Ag_{0.5}$. Labels are explained at the beginning of Sec. III.

	F_d	F_d^H	H_d
$(c/a)_g$ (two layers)	1.632 993		1.633 155
r_{WS} (Bohr)	2.934 354		2.934059
B (GPa)	155.11		154.85
E (mRy)	0		0.077
R		0	0.003
c_s (GPa)		563	547
c_{11} (GPa)	182	256	245
c_{12} (GPa)	137	116	124
c_{13} (GPa)		92	94
c_{33} (GPa)		280	277
c_{44} (GPa)	94	46	47
$c_{66} = (c_{11} - c_{12})/2$ (GPa)		70	61

For the elastic parameters the difference between the results obtained using the two representations is somewhat more pronounced. The difference in the linear compressibilities R involves a first-order derivative of $(c/a)_0$ with respect to the volume. Within both representations, R should be zero. However, R in H_d has a small finite value (0.003). The average deviation obtained between the F_d^H and H_d sets of c_{ij} is 4.5%. The numerical determination of the other elastic parameters, being the second-order derivative of the total energy with respect to the distortions, is computationally demanding. This leads to numerical instabilities discussed in more detail in Sec. III A in Ref. 4. However, within the same representation, the numerical errors are expected to cancel each other. Therefore, in Secs. III B and V, we will refer to the effect of ordering and composition within the same representation (hexagonal), avoiding a direct comparison between the elastic properties of different representations.

B. Effect of long-range order on elastic parameters

Figure 1 shows the two-dimensional total energy surface, $E(V,c/a)$, for the three different hexagonal phases. The total energies per site are plotted using the same reference energy, therefore the figures also indicate the relative stability of the different phases. One can notice that the ordered phase H_o is the stable one. In Table II one can find the total energies per site relative to the fcc (F_d) phase. It is clearly seen that $Pd_{0.5}Ag_{0.5}$ in $L1_1$ layered structure (H_o) has the lowest energy in agreement with the previous theoretical prediction.[5]

Regarding the other bulk parameters (Table II) we can notice that the effect of long-range order is small, but there is a clear trend. The closest values compared to the random fcc phase (F_d) are found in the disordered hexagonal case (H_d), as expected. Increasing the ordering leads to gradually increasing deviations compared to the F_d values. Similar trends can be found for R and c_s as well (Table III).

The data shown in Fig. 1 is analyzed in more detail in Figs. 2 and 3. Figure 2 shows how the equilibrium axial ratio $(c/a)_0$

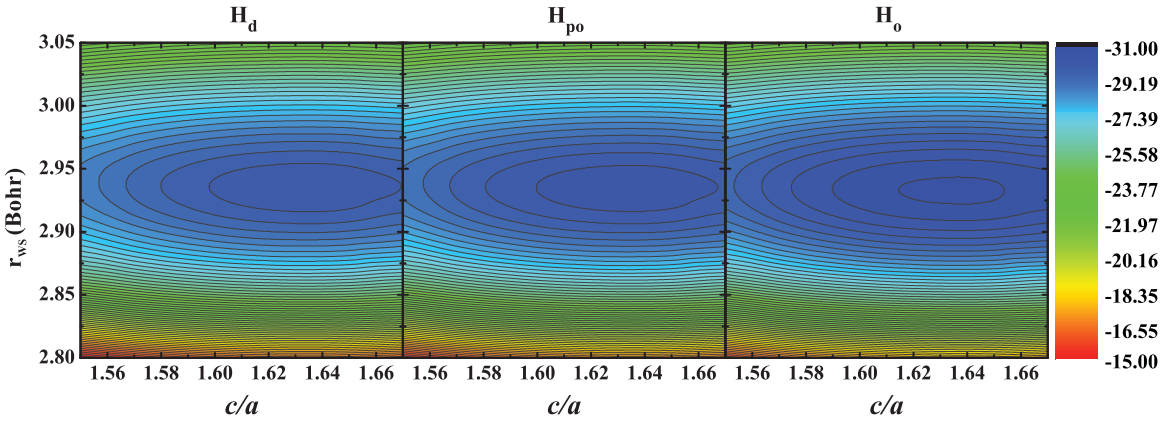

FIG. 1. (Color online) Total energies per site as a function of c/a and r_{WS}. Due to the same reference level, the energy plots indicate the relative stability of the different hexagonal phases. Labels are explained at the beginning of Sec. III.

changes as a function of volume and ordering. For H_d this is close to the ideal c/a ratio leading to a negligible difference between the linear compressibilities along the a and c axis. This is reflected by the small R value in Table III. As we go from the disordered phase to the ordered phase the variations in $(c/a)_0$ become larger. The magnitude of the slope of the $(c/a)_0$ vs r_{WS} curves calculated for the global equilibrium c/a_g increases from H_d to H_o, leading to an increasing R.

We obtained the values of c_s using the second-order derivative of the $E(V,c/a)$ vs r_{WS} curves shown in Fig. 3. The energy scale is the same as in Fig. 1, indicating the relative stability of H_o against the other hexagonal phases.

The effect of ordering on single-crystal elastic constants is shown numerically in Table III. We find the largest ordering effect in the case of c_s (10 GPa, 1%) and the smallest for c_{44} (2 GPa, 1%).

IV. DISCUSSION

Results for the difference in the linear compressibilities (R in Table III) show that our R for H_d is very close to zero, as it should be for the cubic (random) structure. For H_o, R is relatively large and positive. This indicates that the ordered system is anisotropic: it is more compressible along the a axis than along the c axis.

The calculated linear compressibilities along different axes (K_a along the a axis and K_c along the c axis) are shown in Table III. K_a and K_c have negligible differences for H_d, but significant differences for H_o. One should notice that ordering has a small effect on the compressibility along the a axis, but a large effect along the c direction. This effect becomes understandable if we analyze the type of the nearest-neighbor (NN) interactions in the two extreme systems, H_d and H_o. For the disordered phase, there are Pd-Pd, Ag-Ag, and Pd-Ag interactions along the 12 NN with equal probabilities. Since the NN interactions in H_d involve all tree types of bonds, the compressibilities in different directions are expected to be equal. For the ordered case, on the other hand, there are only either Pd or Ag atoms within an atomic layer perpendicular to the c axis. Therefore, the average compressibility in the x-y plane involves the 6 (3 + 3) Pd-Pd and Ag-Ag bonds and, to a lesser extent, also the 6 out-of-plane Pd-Ag bonds. This situation is not so different from that found in the case of H_d, which explains why K_a is not sensitive to the ordering (layering) effect. However, along the c axis the situation is very different: there are only Pd-Ag type of interactions along the c axis for H_o. Therefore, the compressibility is much more affected by the ordering along the c axis. The difference between K_c in different phases $[K_c(H_o) - K_c(H_d)]$ is negative. This suggests that, at fixed volume (equal to the volume of the alloy), the Pd-Ag bonds are somewhat stiffer than the average of the Pd-Pd and Ag-Ag bonds.

Similar anisotropy in the atomic-scale bonding of $Pd_{0.5}Ag_{0.5}$ has been obtained previously also for the $L1_0$

TABLE II. Theoretical (EMTO-PBEsol) bulk parameters [$(c/a)_g$, r_{WS}, B, and E] of $Pd_{0.5}Ag_{0.5}$ alloy for the three hexagonal phases. The energies are shown with respect to the energy of the F_d structure. Labels are explained at the beginning of Sec. III.

	H_d	H_{po}	H_o
$(c/a)_g$ (two layers)	1.633 155	1.633 289	1.635 288
r_{WS} (Bohr)	2.934 059	2.933 526	2.932 235
B (GPa)	154.85	155.59	156.93
E (mRy)	0.077	−0.201	−0.620

TABLE III. Theoretical (EMTO-PBEsol) R, c_s, single-crystal elastic constants and linear compressibilities along a (K_a) and c (K_c) axes of $Pd_{0.5}Ag_{0.5}$ alloy for the hexagonal phases. Labels are explained at the beginning of Sec. III.

	H_d	H_{po}	H_o
R	0.003	0.006	0.017
c_s (GPa)	547	547	537
c_{11} (GPa)	245	247	249
c_{12} (GPa)	124	124	121
c_{13} (GPa)	94	95	98
c_{33} (GPa)	277	279	280
c_{44} (GPa)	47	47	45
c_{66} (GPa)	61	62	64
K_a (1/GPa)	0.002 160		0.002 161
K_c (1/GPa)	0.002 137		0.002 051

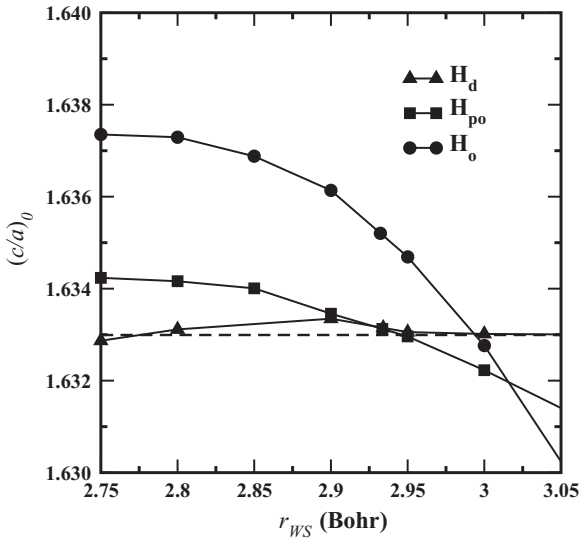

FIG. 2. Equilibrium hexagonal axial ratio $(c/a)_0$ as a function of r_{WS}. Dashed line indicates the ideal c/a value. Labels are explained at the beginning of Sec. III.

(CuAuI-type) structure. For this structure the electron localization function at the Pd site shows stronger bonding in the direction perpendicular to the (100) layers, occupied alternately by Pd and Ag, than along the layers.[29] The structure with Pd and Ag layers is frustrated. The Pd layer is in expanded state and the Ag layer is in compressed state. This is due to the mismatch of the Pd and Ag lattice parameters. Therefore, Pd atoms along the Pd plane are too far from each other to form good bonds. On the other hand, Ag atoms in the Ag plane are too close to each other, leading to increased electronic density between Ag atoms. Pd atoms feel this increased electron density in the Ag plane and try to form bonds toward that. The result is that the Pd bonding along the Pd layer is decreased and, perpendicular to that, it is increased.

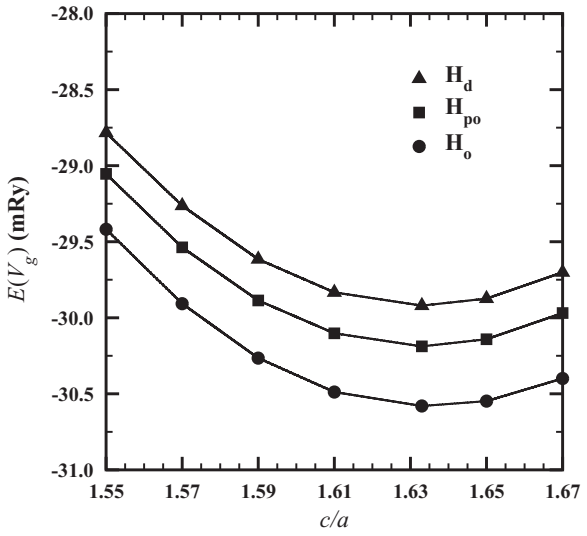

FIG. 3. Energies per site $[E(V_g)]$ at the equilibrium volume as a function of c/a. Energy scale is the same as in Fig. 1. Labels are explained at the beginning of Sec. III.

Since there are no available experimental data on Pd-Ag systems to compare with our results, we recall some similar systems. In the case of Cu_3Au, the experimental results show a negligible ordering effect:[30] the largest change being ∼3% for c_{11} upon ordering. Furthermore, the Debye temperature of Cu_3Au calculated from the measured single-crystal elastic constants increases by 1% upon ordering. The ordering effect is somewhat larger for the ferromagnetic FePd. Depending on the ordered structure, the relative change in the single-crystal elastic constants of FePd ranges between 1% and 16% and the Debye temperature shows an 8% to 10% increase when going from the disordered to the ordered phases.[31] These findings are in line with the present theoretical predictions.

V. CONCLUSION

Applying the transformation rules [Eq. (11)] to the single-crystal elastic constants from Ref. 4, we found that the composition dependence of B, c_{11}, c_{12}, c_{13}, and c_{33} is weakest in the middle of the concentration range ($x = 40$ to 60 at.% Ag). Comparing the effects of composition change and ordering it turned out that the effect of ±5% change in composition around $Pd_{0.5}Ag_{0.5}$ is 4.2, 4.9, 2, 5.6, 1.2, and 1.3 times larger for B, c_{11}, c_{12}, c_{33}, c_{44}, and c_{66}, respectively, than the ordering effect. Based on the above analysis, we conclude that ordering does not significantly affect the bulk and elastic properties of $Pd_{0.5}Ag_{0.5}$. We believe that, taking into account the long-range order, the previously discussed peculiar composition dependence of the properties of Pd-Ag alloys discovered in Ref. 4 will not change, and it is justified to use the random fcc model in this particular case.

ACKNOWLEDGMENTS

The Swedish Research Council, the Swedish Energy Agency, the Turku University Foundation (No. 7743), and the Hungarian Scientific Research Fund (research project OTKA 84078) are acknowledged for financial support. NSC-Matter, UPPMAX, and the Finnish IT Center for Science (CSC) are acknowledged for the computer resources.

APPENDIX

In our previous work[4] we calculated the elastic constants of random $Pd_{0.5}Ag_{0.5}$ for the fcc phase using the conventional coordinate system of cubic lattices. In cubic systems there are three independent elastic constants. Random fcc $Pd_{0.5}Ag_{0.5}$ can be described in a hexagonal phase, too, when the c axis is oriented along the fcc [111] direction. For the hexagonal phase there are five elastic constants defined with respect to the hexagonal coordinate axes. The five hexagonal elastic constants can be expressed in terms of the cubic ones applying the tensor transformation rules to the components of the fourth-rank elastic tensor.

A. Euler's rotation theorem

We applied Euler's rotation theorem[32] to obtain the elements of the tensor transformation matrix. The rotation of the coordinate system can be described using the three Euler angles. Using Euler angles the elements of the rotation matrix

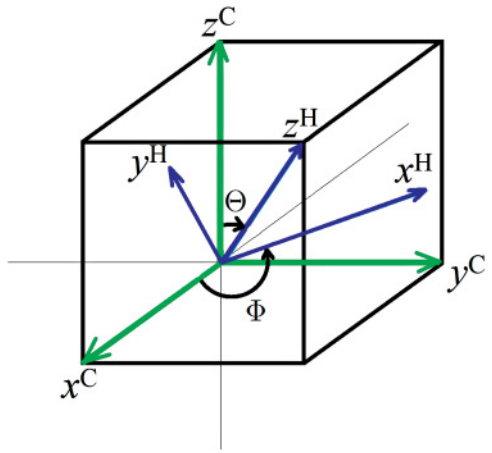

FIG. 4. (Color online) Euler's rotation applied to the fcc phase. Green (lighter) arrows indicate the cubic (x^C, y^C, z^C) coordinate axes and blue (darker) arrows show the hexagonal (x^H, y^H, z^H) axes.

(T) can be obtained by applying different conventions. The most common definition is the so-called "x-convention," which has the following steps (see Fig. 4 for notations):

(1) first, we rotate the system by an angle Φ around the z^C axis;

(2) the next rotation is by an angle Θ around the x^H axis;

(3) the final rotation is by an angle Ψ about the new z^H axis.

The involved rotations are counterclockwise rotations. The elements of the rotation matrix according to the "x-convention" can be defined as follows:

$$T = \begin{pmatrix} T_{11} & T_{12} & T_{13} \\ T_{21} & T_{22} & T_{23} \\ T_{31} & T_{32} & T_{33} \end{pmatrix}, \tag{A1}$$

where

$$\begin{aligned} T_{11} &= \cos\Psi\cos\Phi - \cos\Theta\sin\Phi\sin\Psi, \\ T_{12} &= \cos\Psi\sin\Phi + \cos\Theta\cos\Phi\sin\Psi, \\ T_{13} &= \sin\Psi\sin\Theta, \\ T_{21} &= -\sin\Psi\cos\Phi - \cos\Theta\sin\Phi\cos\Psi, \\ T_{22} &= -\sin\Psi\sin\Phi + \cos\Theta\cos\Phi\cos\Psi, \\ T_{23} &= \cos\Psi\sin\Theta, \quad T_{31} = \sin\Theta\sin\Phi, \\ T_{32} &= -\sin\Theta\cos\Phi, \quad T_{33} = \cos\Theta. \end{aligned} \tag{A2}$$

In the present case, $\Phi = 135^\circ$, $\Theta = \arctan\sqrt{2}$ and $\Psi = 0^\circ$ yield the matrix given in Eq. (9).

[1] *Binary Alloy Phase Diagrams*, edited by T. B. Massalski (ASM International, Metals Park, 1992).
[2] E. Bruno, B. Ginatempo, and E. S. Giuliano, Phys. Rev. B **52**, 14544 (1995).
[3] E. Bruno, B. Ginatempo, and E. S. Giuliano, Phys. Rev. B **52**, 14557 (1995).
[4] E. K. Delczeg-Czirjak, L. Delczeg, M. Ropo, K. Kokko, M. P. J. Punkkinen, B. Johansson, and L. Vitos, Phys. Rev. B **79**, 085107 (2009).
[5] S. Müller and A. Zunger, Phys. Rev. Lett. **87**, 165502 (2001).
[6] P. Hohenberg and W. Kohn, Phys. Rev. B **136**, 864 (1964).
[7] A. V. Ruban, S. I. Simak, P. A. Korzhavyi, and B. Johansson, Phys. Rev. B **75**, 054113 (2007).
[8] O. K. Andersen, O. Jepsen, and G. Krier, in *Lectures on Methods of Electronic Structure Calculation* (World Scientific, Singapore, 1994), p. 63.
[9] L. Vitos, H. L. Skriver, B. Johansson, and J. Kollár, Comp. Mat. Sci. **18**, 24 (2000).
[10] L. Vitos, Phys. Rev. B **64**, 014107 (2001).
[11] L. Vitos, I. A. Abrikosov, and B. Johansson, Phys. Rev. Lett. **87**, 156401 (2001).
[12] L. Vitos, *The EMTO Method and Applications in Computational Quantum Mechanics for Materials Engineers* (Springer-Verlag, London, 2007).
[13] W. Kohn and L. J. Sham, Phys. Rev. **140**, A1133 (1965).
[14] O. K. Andersen, C. Arcangeli, R. W. Tank, T. Saha-Dasgupta, G. Krier, O. Jepsen, and I. Dasgupta, Mater. Res. Soc. Symp. Proc. **491**, 3 (1998).
[15] P. Soven, Phys. Rev. **156**, 809 (1967).
[16] B. L. Györffy, Phys. Rev. B **5**, 2382 (1972).
[17] J. Kollár, L. Vitos, and H. L. Skriver, *Electronic Structure and Physical Properties of Solids: the Uses of the LMTO Method in Lecture Notes in Physics*, edited by H. Dreyssé (Springer-Verlag, Berlin, 2000), p. 85.
[18] A. Taga, L. Vitos, B. Johansson, and G. Grimvall, Phys. Rev. B **71**, 014201 (2005).
[19] Z. Nabi, L. Vitos, B. Johansson, and R. Ahuja, Phys. Rev. B **72**, 172102 (2005).
[20] L. Vitos, P. A. Korzhavyi, and B. Johansson, Nat. Mater. **2**, 25 (2003).
[21] B. Magyari-Köpe, G. Grimvall, and L. Vitos, Phys. Rev. B **66**, 064210 (2002); **66**, 179902 (2002).
[22] B. Magyari-Köpe, L. Vitos, and G. Grimvall, Phys. Rev. B **70**, 052102 (2004).
[23] L. Vitos, P. A. Korzhavyi, and B. Johansson, Phys. Rev. Lett. **88**, 155501 (2002).
[24] L. Huang, L. Vitos, S. K. Kwon, B. Johansson, and R. Ahuja, Phys. Rev. B **73**, 104203 (2006).
[25] P. A. Korzhavyi, A. V. Ruban, I. A. Abrikosov, and H. L. Skriver, Phys. Rev. B **51**, 5773 (1995).
[26] J. P. Perdew and Y. Wang, Phys. Rev. B **45**, 13244 (1992).
[27] J. P. Perdew, A. Ruzsinszky, G. I. Csonka, O. A. Vydrov, G. E. Scuseria, L. A. Constantin, X. Zhou, and K. Burke, Phys. Rev. Lett. **100**, 136406 (2008).
[28] H. Zhang, M. P. J. Punkkinen, B. Johansson, S. Hertzman, and L. Vitos, Phys. Rev. B **81**, 184105 (2010).
[29] K. Kokko, R. Laihia, M. Alatalo, P. T. Salo, M. P. J. Punkkinen, I. J. Väyrynen, W. Hergert, and D. Ködderitzsch, Phys. Rev. B **60**, 4659 (1999).
[30] P. A. Flinn, G. A. McManus, and J. A. Rayne, J. Phys. Chem. Solids **15**, 189 (1960).
[31] T. Ichitsubo and K. Tanaka, J. Apl. Phys. **96**, 6220 (2004).
[32] [http://mathworld.wolfram.com/EulerAngles.html].